High-temperature XRD investigations on phase transformations

R. Montanari

The first part of this paper briefly describes how X-ray diffraction (XRD) is used for the determination of phase diagrams and gives some examples of particular interest. The attention is focused on in situ XRD experiments, i.e. performed directly at the high temperatures where phase transformations take place. The related experimental problems are presented and discussed.
Furthermore, high temperature XRD offers the possibility to investigate structural aspects of phase transformations involving both solid and liquid. In order to illustrate the precursor phenomena occurring in melting and solidification and the correlations between the structures of solid and liquid phases, the second part of the paper presents some results obtained from investigations on pure indium (99.99 wt%) and In90-Sn10 alloy.

Parole chiave: high temperature X-ray diffraction, phase diagrams, phase transformation, melting, solidification

INTRODUCTION

For the great importance of phase diagrams in metallurgy and materials science, a lot of work has been devoted to their determination. Thermal analysis and microscopic examination are the experimental techniques more used in this kind of investigations. X-ray diffraction (XRD) supplements these methods and, permits, in addition, to find the crystal structures of the solid phases involved.
Many phase diagrams are determined today by combining the three techniques, which exhibit different sensitivity in different portions of phase diagrams. For instance, the best results in finding liquidus and solidus curves, peritectic and eutectic horizontals are obtained by thermal analysis, which, conversely, could fail when very slow solid state reactions and small heat effects are involved. Solvus curves, peritectoid and eutectoid horizontals are best determined by microscopic examination or XRD.
This paper gives some examples of XRD applications to phase diagrams determination and discusses the related experimental problems. Furthermore, XRD offers the possibility to investigate structural aspects of phase transformations involving both solid and liquid phases.
Although XRD is fundamental for investigating phase transformations in solids under high pressures, this aspect is not considered here.

XRD AND PHASE-DIAGRAM DETERMINATION

To understand how XRD can be used for determining the features of a phase diagram, it is worth to recall some general principles.
Each phase of an alloy produces its own diffraction pattern independently of the presence of any other phase. So, the XRD spectrum of a multi-phase alloy is the superposition of the patterns of any single phase. The relative amount of each phase is proportional to the integrated intensity under the corresponding pattern.

R. Montanari
INFM-Dipartimento di Ingegneria Meccanica- Università di Roma-Tor Vergata, Roma

Memoria presentata al seminario: Phase transformations and phase diagrams, Milan 23 settembre 2003

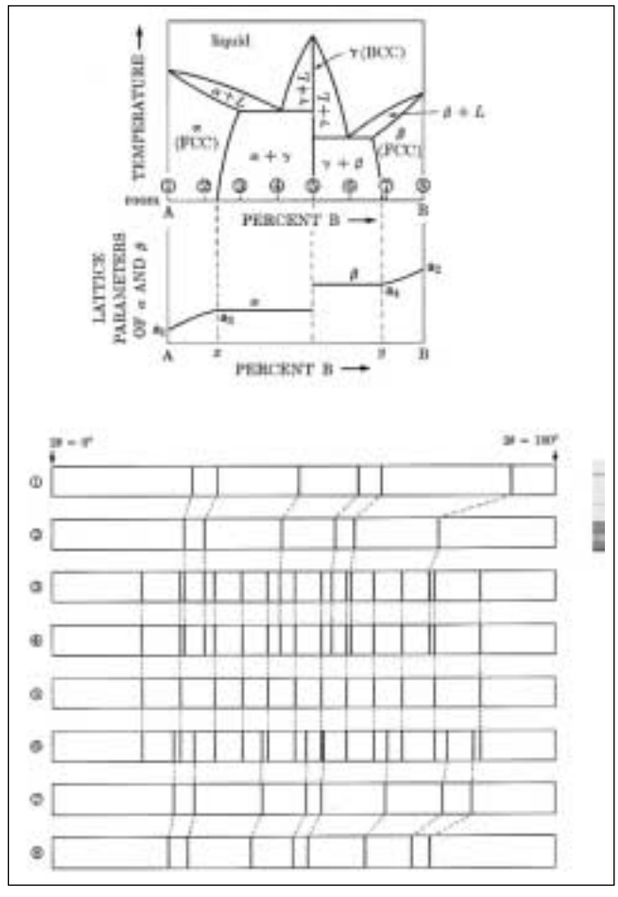

Fig.1- Phase diagram of an hypothetical binary alloy and XRD patterns of alloys 1 to 8 (ref.[1]).

Fig.1- Diagramma di fase di un' ipotetica lega binaria e figure di diffrazione X delle leghe 1-8 (ref.[1]).

In the case of a single-phase region any variation of composition has the effect of changing the cell parameters thus it causes a shift of angular peak positions. An example taken from the classical book of Cullity [1] is shown in fig.1.
In the following some XRD applications to phase diagram determination are presented.

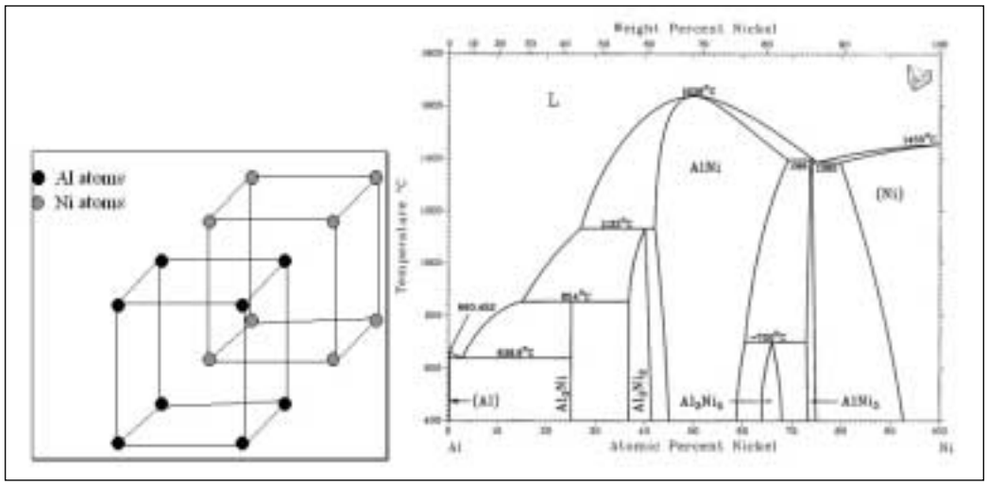

Fig.2- B2 cell of the Al50-Ni50 alloy (left), Al-Ni phase diagram (right).

Fig.2 Cella B2 della lega Al50-Ni50 (sinistra), diagramma di fase Al-Ni (destra).

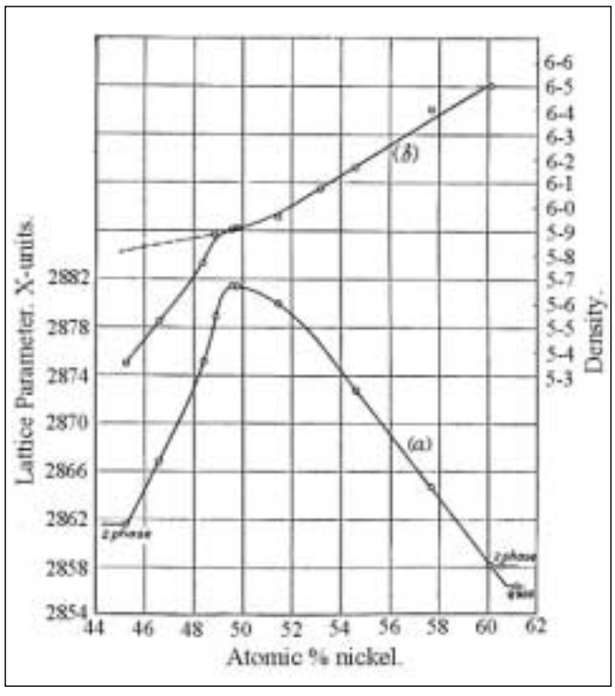

Fig.3- Lattice parameter (a) and density (b) of the Al-Ni β phase vs. Ni content (ref.[5]).

Fig.3- Parametro reticolare (a) e densità (b) della fase β del sistema Al-Ni in funzione del contenuto di Ni (ref.[5]).

Ordering in substitutional solid solutions

XRD is a fundamental technique in investigating ordering. This type of solid state transformation takes place in a lot of metal systems and can produce a large number of structures. The transition from random to ordered lattice in a given alloy is revealed by the appearing of superlattice reflections in the XRD pattern. Since superlattice peaks have low intensities, only low angle reflections are usually detected.
The long-range order parameter S, which indicates the ordering degree, is obtained by comparing the integrated intensities of superlattice and corresponding fundamental reflections, e.g. the superlattice {100} and the fundamental {200} reflections in a bcc structure.
A rough estimate of the mean size L of ordered domains can be determined from the expression:

$$L = \lambda / \cos\theta \; \beta(2\theta) \qquad (1)$$

where λ is the wavelength, θ is the Bragg angle of a superlattice reflection and β(2θ) is the half height linewidth expressed in radians.
Furthermore, XRD permits to determine: 1) the fraction of lattice sites occupied by anti-site atoms (an example is given in [2] for Fe-Al system), 2) the lattice site occupation of third elements added to a binary ordered alloy [3], 3) the vacancy content in defect type ordered solid solutions [4]. The last point concerns only few metal systems. The best known example is the intermediate β solution in the Al-Ni system (see fig.2).
At the stoichiometric composition Al50-Ni50 we have the B2 structure formed by two interlaced cubes shown in fig.2 (left): Al atoms are located at the corners of one cube and Ni atoms at the corners of the other cube. On the Ni-rich side of the ideal composition some Al atoms are randomly replaced by those of Ni. Since Ni atoms are smaller and heavier than those of Al, the increase of Ni content causes the density to increase and lattice parameter to decrease. On the Al-rich side one would expect the contrary. However, this is not the case: it has been demonstrated by XRD [5] that both lattice parameter and density drop on the Al-rich side (fig.3). The anomalous trends can be explained by supposing that the Ni positions which would normally have been occupied by Al atoms in excess remain unfilled, i.e. they become vacant sites.
Superlattice reflections of a binary alloy are generally proportional to $(f_A - f_B)^2$, where f_A and f_B are the atomic scattering factors of metals A and B. Therefore, if the atomic numbers Z_A and Z_B are very close, the intensity of these peaks could be so low to be undetectable. For instance, this is the case of the system Cu-Zn (Z_{Cu} = 29, Z_{Zn} = 30), which exhibits an ordering transition from the disordered β phase to the B2 ordered β' phase.
To overcome this drawback it is possible to use a proper X-ray wavelength λ, i.e. very close to the absorption edge of one of the scattering atoms. The electron oscillations are disturbed because the radiation to scatter has a frequency near that at which the electrons are ejected from the atom and f value undergoes a sharp decrease (anomalous dispersion). Under these conditions the trends of f vs. λ for elements A and B exhibit steep variations and the difference $(f_A - f_B)$ results strongly increased causing higher intensities of superlattice peaks. In the case of Cu-Zn, superlattice reflections can be clearly detected if the Zn-Ka radiation is employed.

Solvus curves

A solvus curve forms the boundary between a single-phase solid region and a two-phase solid region; the single-phase may be a primary or an intermediate solid solution.
The XRD methods for determining the solvus curve are two:
- the disappearing phase method,
- the parametric method.

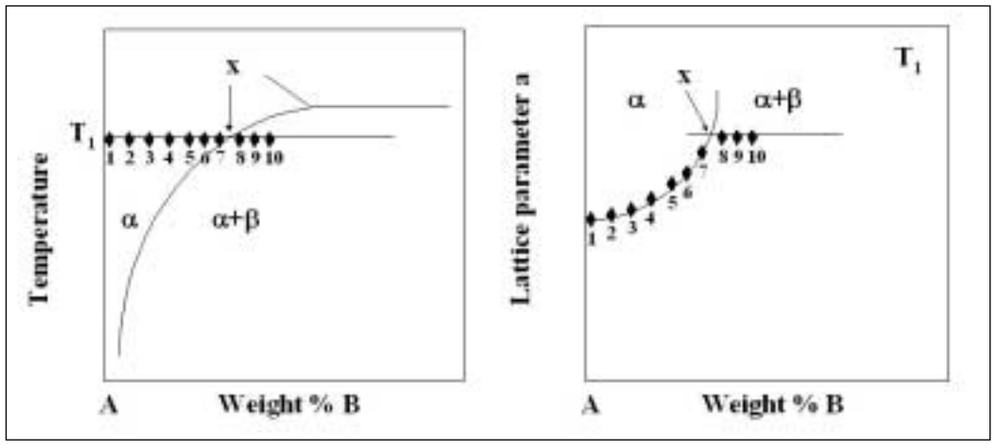

Fig.4- (Left) Hypothetical phase diagram with solvus curve. (Right) Lattice parameter a vs. B content for alloys 1-10 (parametric method).

Fig.4- (Sinistra) Ipotetico diagramma di fase con una curva di solvus. (Destra) Parametro reticolare a in funzione del contenuto di B per le leghe 1-10 (metodo parametrico).

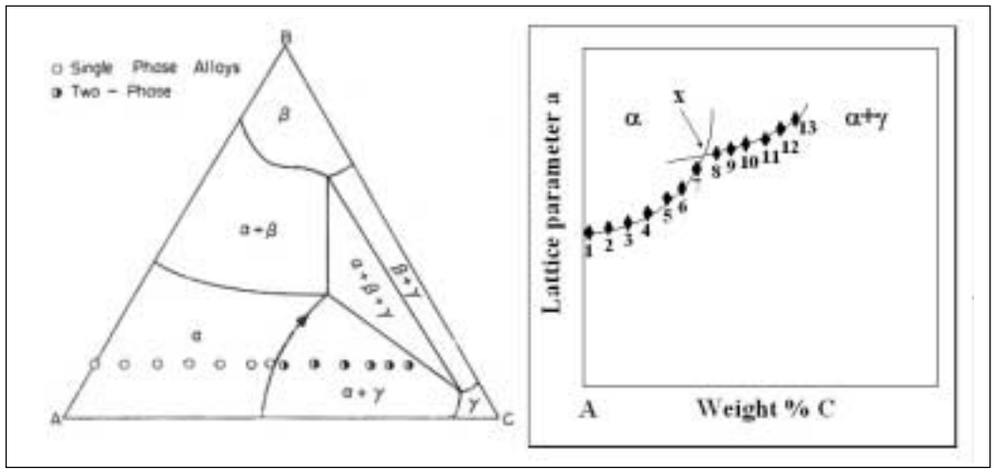

Fig.5- (Left) Hypothetical ternary phase diagram. (Right) Lattice parameter a vs. C content (B is constant) for alloys 1-13 indicated by dots in the diagram on the left.

Fig.5- (Sinistra) Ipotetico diagramma di fase ternario. (Destra) Parametro reticolare a in funzione del contenuto di C (B è costante) per le leghe 1-13 indicate dai punti nel diagramma a sinistra.

Let us consider a binary system formed by metals A and B. Fig.4 (left) schematically shows the phase diagram. At a given temperature T_1 the alloys with B content higher than x exhibit a biphasic structure and the relative amounts of the phases α and β can be calculated by the lever law.
To determine the solvus curve between the α and the (α+β) regions it is necessary to find for each temperature T the corresponding point x.
The disappearing phase method consists in measuring the ratio I_β/I_α between two prominent reflections of the phases α and β for a certain number of alloys with decreasing B content, prepared at the temperature T. The ratio I_β/I_α decreases as B content decreases so the point x is determined by extrapolating to zero the ratio value (phase β is not more present in the mixture). The other points of solvus curve are determined in analogous way by testing different sets of samples prepared at other temperatures.
The precision of the method mainly depends on the XRD sensitivity in detecting small amounts of the second phase β in the mixture. This sensitivity is not constant but varies with the couple of metals A and B. The intensity of a diffraction line is a function of the atomic scattering factor f, which is in turn almost proportional to the atomic number Z. So, if the atomic numbers Z_A and Z_B are close, an amount of about 1 percent of the second phase can be revealed. Conversely, in the extreme case that Z_A differs from Z_B of 70 or more units, also 50 percent of β phase could produce diffraction lines of negligible intensities, i.e. comparable with background. Of course, the method is useless under these circumstances.
Anyway, if the biphasic region is very narrow, of the order of few percents, it is always possible to determine x with sufficient precision. Even if atomic numbers of A and B are quite different, the compositions of α and β are similar so as their diffraction powers.
Since the trend of I_β/I_α vs. weight percent B is not linear, it is necessary to have many experimental points near the boundary to get sufficient accuracy.
The parametric method is based on the fact that in the solid single-phase region the cell parameters change as a function of the composition. For simplicity, let us consider a cubic system where only one cell parameter is involved. As B content in the alloy increases, the cell parameter a increases if the size of B atoms is larger than that of A atoms, decreases in the opposite case.
Fig.4 (right) shows the trend of a vs. B content for a set of samples brought at equilibrium at the temperature T_1 where the α region has a large extent, rapidly cooled to room temperature and tested by XRD. The curve exhibits two branches: in the first part the lattice parameter a increases as B content increases, in the second part it remains constant.
In the single-phase region an increase of B content produces a lattice expansion of the α phase. When the α phase lattice is not more able to accomodate the atoms of type B, further increase of B produces the precipitation of the β phase. In the biphasic region, the increase of B increases the amount of β phase in the mixture while the lattice parameter a of α phase remains unchanged (second branch of the curve). The point x is given by the intersection of the two branches of the parametric curve.
To find the points of the solvus at different temperatures, it is sufficient to prepare just one alloy at different temperatures, measure a and use the curve in fig.4 (right) as a master curve.
The parametric method can be used to determine the boundary between a single-phase and a two-phase region in ternary systems. In the hypothetic case of the diagram shown in fig.5 (left) the line separating α and (α+γ) regions has to be determined.

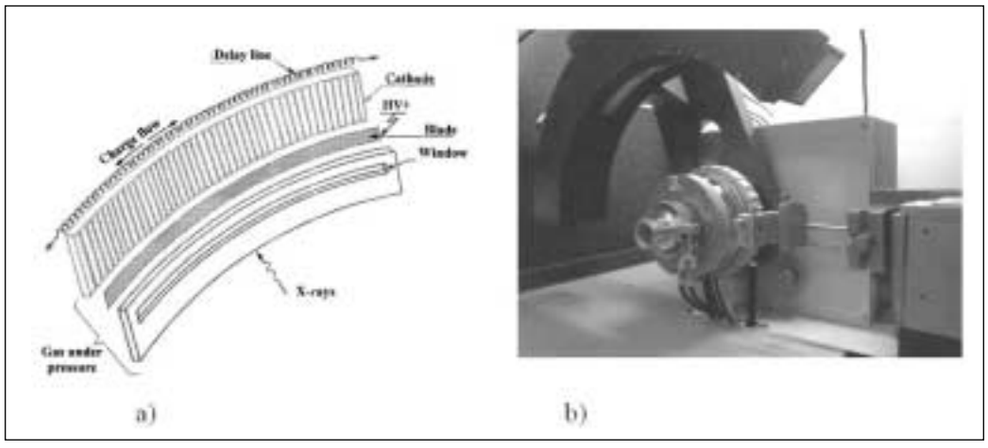

Fig.6- Layout of the curved position-sensitive detector (a); T.A.D. instrument with high temperature camera (b).

Fig.6- Schema del rivelatore curvo con sensibilità di posizione (a); apparecchiatura T.A.D. con camera ad alta temperatura (b).

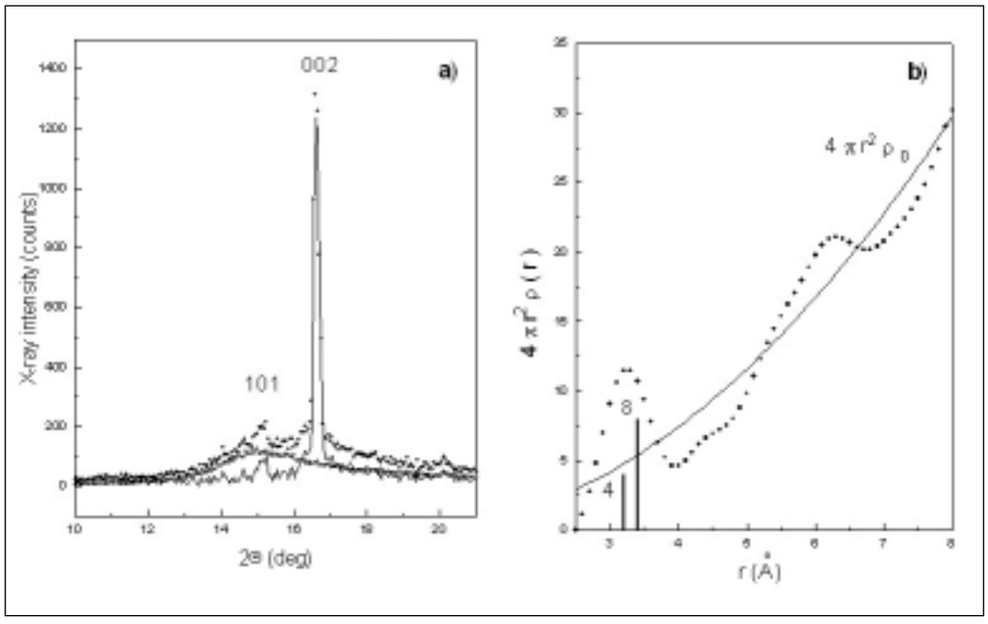

Fig.7- a) The diffraction pattern of indium collected during melting (black dots) is the sum of liquid (open circles) and solid (continuous line) contributions. b) The RDF curve, $4\pi r^2 \rho(r)$ vs. r, obtained from the liquid diffraction pattern in a). Bars indicate the distribution of 1st and 2nd neighbours in crystalline indium.

Fig.7- a) Lo spettro di diffrazione dell'indio acquisito durante la fusione (punti neri) è la somma dei contributi dovuti al liquido (cerchi) e al solido (linea continua). b) Curva RDF, $4\pi r^2 \rho(r)$ vs. r, ottenuta dalla figura di diffrazione del liquido in a). Le barre indicano la distribuzione dei primi e secondi vicini nel cristallo dell'indio.

The lattice parameter of a set of alloys with compositions parallel to one side of the ternary triangle exhibits a trend like that in fig.5 (right). In the two-phase region the lattice parameter is not constant as in binary systems, however the curve is always formed by two branches with different slopes and the composition corresponding to the slope change identifies the point x of the curve separating α and $(\alpha+\gamma)$ regions.

HIGH TEMPERATURE XRD

Usually X-ray experiments are performed on alloys equilibrated at a given temperature, then quenched down to room temperature to freeze the structure present at high temperature. If, notwithstanding the rapid cooling, they transform it is necessary to record the spectra directly in temperature. In situ XRD is decisive in those cases where the high temperature phase cannot be quenched and preserved at low temperature.

The experiments can be performed by means of a high-temperature (HT) X-ray camera mounted on a standard diffractometer. This conventional technique is good for monitoring phenomena when the kinetics of transformation is relatively slow. On the other hand, fast kinetics require fast data acquisition, so counting time for each step should be kept short and does not guarantee a sufficient accuracy. Two possible solutions can be adopted to overcome this drawback:

1- to operate by standard diffractometry employing fast detectors,

2- to operate by Time Analysis Diffractometry (T.A.D.).

Fast detectors available today are about hundred times faster than standard solid-state detectors. Of course, measurements with fast detectors involve longer acquisition time to collect spectra over a larger 2θ range.

The experimental apparatus for T.A.D. substantially consists of a side-window position-sensitive counter and a multichannel analyser (MCA). A sketch of the detector is shown in fig.6a).

The counter, which is filled with a gas mixture under pressure, is placed under an intense electrical field. The anode of the counter is a curved blade, the cathode is divided into equal parts connected by a delay line, which permits to determine the position of the photons causing charge pulses. The pulses are then converted to digital form, analysed and sorted by the MCA. Therefore, the number of counts (pulses) stored in MCA memory is a function of the 2θ position where they originated. The diffraction pattern is obtained by displaying the MCA memory content. The 2θ angular resolution (0.03°) is comparable with that of a standard diffractometer (0.005°). The geometry of the device resembles that of a Debye-Scherrer camera but the resolution is higher because a proportional counter replaces the film strip. The whole diffraction pattern is recorded simultaneously across a wide angular range. Fig.6 b) shows the front view of the HT camera and the curved detector, which covers a 2θ angu-

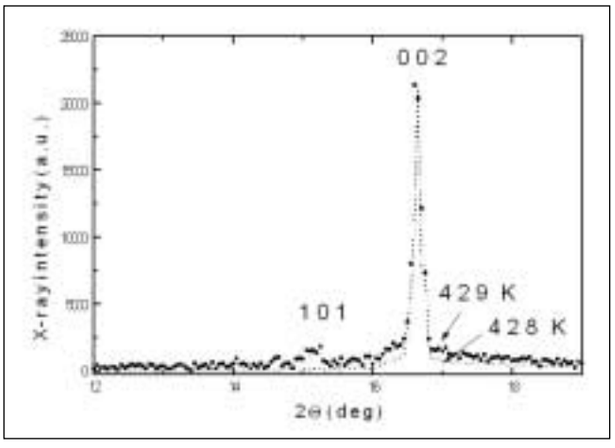

Fig.8- The XRD pattern recorded at 428 K, just below T_M, is compared with the contribution from solid to the overall pattern recorded at T_M.

Fig.8- Lo spettro XRD acquisito a 428 K, immediatamente sotto T_M, è confrontato con il contributo del solido alla figura di diffrazione complessiva acquisita a T_M.

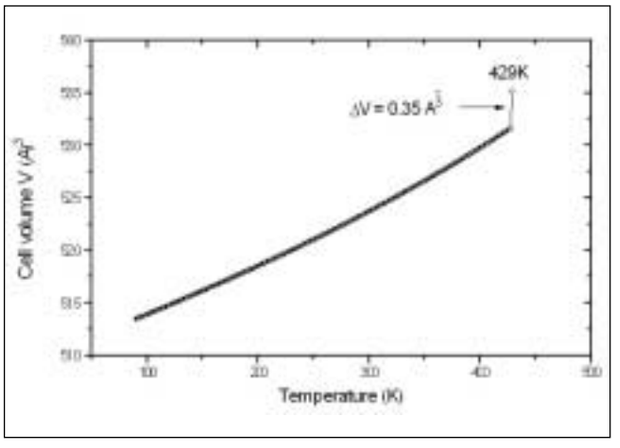

Fig.9- Cell volume of indium vs. temperature.

Fig.9- Volume di cella dell'indio in funzione della temperatura.

lar range of 120° and allows to record the whole diffraction pattern in few seconds.
In HT X-ray cameras the commonly used heater consists of a Pt plate. The sample is allocated on the heater strip thus great attention has to be paid to temperature calibration because thermal gradients between heater and sample or inside the sample could seriously affect the results [6].
In some cases the Bragg-Brentano geometry could give rise to important errors. For instance, during peritectic decomposition the solid fraction, which is usually denser, can sink below the penetration depth of X-rays. This drawback can be overcome by employing a transmission geometry (Debye-Scherrer) with the sample sealed in a cylindrical rotating capillary. An example is shown in ref. [7]. If the material has a high absorption coefficient, high energy X-rays are required for such kind of geometry.

PRECURSOR EFFECTS OF PHASE TRANSFORMATIONS

An interesting aspect of phase transformations regards the structural changes which immediately precede them. In this paper the attention is focused on melting and solidification of pure metals and binary alloys. In particular, Indium and its alloy In90-Sn10 are considered to give some examples of precursor phenomena. The reported data are taken from previous papers of the author et al. [8-10].
A lot of experimental data have been accumulated about the peculiarities of melting and solidification of pure metals and alloys. (e.g. see the review in ref.[11]). Both the phase transformations in pure metals involve a discontinuous jump in thermodynamic parameters such as enthalpy and (usually) volume even if precursor effects due to structural changes occur on either side of the discontinuity. XRD permits to investigate the structural aspects in solid and liquid, which are of the utmost importance for the explanation of the great variety of behaviours observed in different metals and to validate theoretical models.
Let us consider now melting and solidification of pure indium.
The XRD spectrum recorded at T_M is the overlapping of diffraction patterns due to liquid and solid phases. As shown in fig.7 a), the two contributions can be separated, then examined.
The radial distribution function (RDF) curve obtained from the liquid contribution of fig.7 a) is plotted in b). It oscillates above and below the average density curve $4\pi r^2 \rho_0$. Bars indicate the distribution of 1st and 2nd neighbours in crystalline indium. RDF exhibits the first peak centred at 3.3 Å. Indium is tetragonal body centred: 1st neighbours (4 atoms) are at a distance of 3.25 Å and 2nd neighbours (8 atoms) at 3.38 Å. Therefore, shell radii of the 1st and 2nd neighbours in solid are very close to the mean distance of nearest neighbours in liquid as obtained from the RDF.
When compared to the spectrum recorded at a temperature (428 K) just below T_M, the contribution due to solid phase exhibits some important features (fig.8).

1- The {101} reflection, absent in the spectrum at 428 K, appears at 429 K even if its intensity is relatively low. The presence of the {101} reflection involves an abrupt re-orientation of the diffracting solid, which accompanies or immediately precedes the formation of the first liquid.
2- The {002} line profile is broadened in particular in the lower part of the peak.
3- During melting the {002}peak shifts towards lower angles.

Thermal expansion of indium is unusual because the c-axis passes through a maximum near room temperature. The following equations give a and c, expressed in Å, as a function of the absolute temperature T:

$$a = 3.2182 + 8.47 \times 10^{-5} T + 3.61 \times 10^{-10} T^3 \quad (2)$$

$$c = 4.9201 + 15.15 \times 10^{-5} T - 6.64 \times 10^{-10} T^3 \quad (3)$$

The lengths of c-axis measured at different temperatures up to 428 K in the present work are substantially in agreement with that prediction but they turn away when the first liquid forms. The observed peak shift corresponds to a remarkable change in {002} interplanar spacing (d_{002} = 2.4494 Å at 428 K, d_{002} = 2.4568 Å at 429 K) thus it involves an abrupt increase of the c-axis. The same phenomenon has been observed in another set of samples with {101} texture. Combining the data obtained from samples with {002} and {101} texture, the lattice cell volume vs. temperature has been calculated (fig.9). The abrupt volume increase ΔV observed at melting point is 0.35 Å^3. This can be explained by the occurrence of an abnormal increase of vacancy concentration in the solid. In fact, the main effect of vacancies on crystal lattice consists in its isotropic dilatation with consequent increase of all the interplanar spacings, which is evidenced by a general shift of XRD reflections towards lower angles.
The vacancy concentration C_{429} at 429 K has been estimated as:

$$C_{429} = C_{428} + \Delta C \quad (4)$$

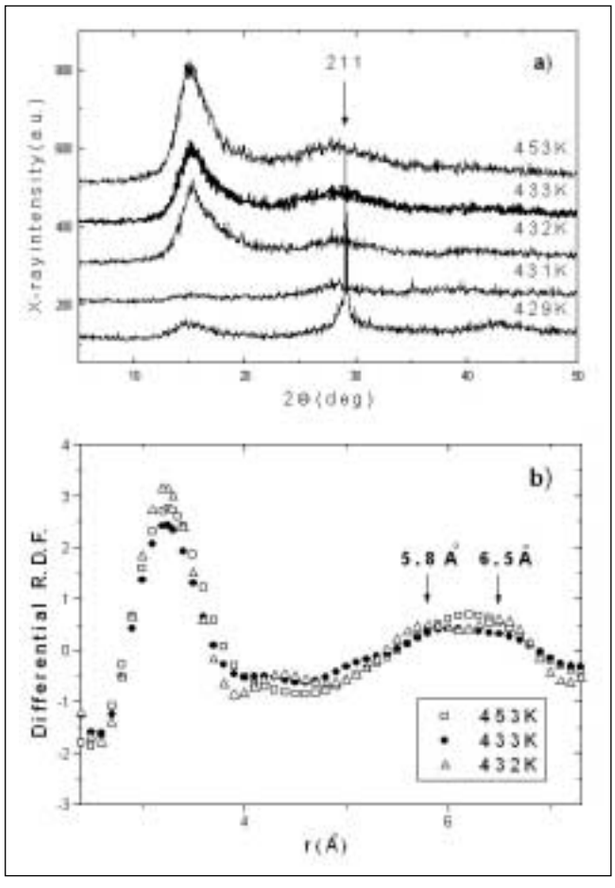

Fig.10– a) XRD spectra of liquid indium recorded at different temperatures during cooling to T_M. b) Differential RDF curves of liquid indium obtained from diffraction patterns in a).

Fig.10– a) Spettri XRD di indio liquido acquisiti a diverse temperature durante il raffreddamento fino a T_M. b) Curve RDF differenziali ottenute dalle figure di diffrazione in a).

where C_{428} is the vacancy concentration of thermodynamic equilibrium at 428 K and ΔC is the increase giving rise to the cell volume expansion ΔV shown in fig.11.
Being $C_{428} = 1.12 \times 10^{-4}$ and $\Delta C = 6.74 \times 10^{-3}$, the vacancy concentration C_{429} of the solid in presence of its liquid results to be $\approx 6.85 \times 10^{-3}$. Details of the calculation may be found in [10].
Beside lattice expansion, an abnormal increase of vacancies at T_M should involve extremely favourable conditions for vacancy clustering. Due to higher concentration and migration velocity, vacancies usually tend to aggregate forming complex defects as temperature increases (see for instance ref.[12]). The broadening of XRD peaks, in particular in the lower part, is consistent to vacancy clustering in small dislocation loops, which produce a diffuse scattering affecting the tails of diffraction profiles [13].
As shown in fig.8, the {101} peak appears when the first liquid forms. To explain the change two hypothesis connected to different morphologies (diffuse or sharp) of the solid-liquid (S-L) interface can be considered.
In the case of a diffuse interface, liquid advances in the solid along preferential directions and solid blocks, detached from the bulk, may be drag away by the liquid. This process produces a re-orientation of the blocks, which can give rise to the appearing of new diffraction peaks.
If the S-L interface is sharp, the presence of the {101} peak may be explained by a sudden texture change in the solid phase. Due to preliminary treatment the examined material has a low dislocation density. Therefore, the driving force for recovery and recrystallization is low and the possible texture change (2nd hypothesis) is ascribable to grain growth, which is made easier by the initial strong texture [14]. In this case the presence of {101} peak is due to the growth of grains with this orientation at expenses of those of [002] orientation. Since grain growth is a thermally activated process, the abrupt appearing of {101} peak is a further indication of the abnormal increase of vacancy concentration observed immediately before melting. The enhancement of boundary mobility by a vacancy flux or supersaturation has been extensively discussed in several reviews.
Anyway, regardless the interface morphology, the lattice planes facing the first formed liquid are the {101} and {002} planes, which allocate 1st and 2nd neighbours with shell radii very close to the mean distance of next neighbours in liquid. On the ground of present results, a correlation between the structures of solid and liquid seems to exist.
Let us consider now what happens during the solidification. XRD patterns of liquid indium have been recorded at decreasing temperatures to study the structures in the melt approaching T_M. Fig.10 a) shows the XRD spectra collected during cooling to T_M where the first solid forms with a strong [211] orientation.
The diffraction pattern recorded at 431 K, i.e. immediately before solidification, shows an anomalous trend: the second maximum is more intense than the first one. The differential RDF curves obtained from diffraction patterns in fig.10 a) are plotted in b).
Also the experiments of solidification seem to confirm that the structures of liquid and solid are correlated. The split of the 2nd RDF maximum indicates that a structural change in the liquid phase precedes the solidification. Atom clusters form with mean distances corresponding to those of nearest neighbours in those planes, {211}, which will result to face the liquid. The distance between nearest neighbours on {211} planes of Indium is 5.9 Å. These are low-atomic-density planes and grow faster than the close-packed planes as {002}. As a consequence, slow-growing close-packed faces are the most developed ones, and that will determine the final texture.
Similar indication on structural changes preceding and accompanying phase transformations can be achieved also for the alloys. In the following the solidification of the In90-Sn10 alloy will be examined.
In fig.11 (left) the differential RDF curve, $\Sigma_{UC} K_m . 4\pi r^2 [\rho_m(r) - \rho_0(r)]$, of In90-Sn10 alloy recorded at 457 K (A) and 420 K (B) is compared with that of indium 99.99% (C) at 430 K. As shown by the In-Sn phase diagram of fig.11 (right), 420 K for In90-Sn10 and 430 K for indium are temperatures just above those at which the first solid begins to separate from the liquid.
The first peak is a little broader in A and B than in C because it is the overlapping of the Sn-Sn and In-In nearest neighbours components, centred at 3.2 and 3.3 Å respectively. The two components are too close to be distinguished.
The origin of peaks at 5.8 and 6.5 Å in the curve of indium (C) has been already discussed before. Both the curves (A and B) of In90-Sn10 alloy exhibit the same peaks of curve C even if they are more pronounced and a little shifted. In addition, curves A and B show a subsidiary peak at 4.4 Å due to In-Sn nearest neighbours, which is of negligible intensity in the curve of indium (C). From the comparison between curves A and B it possible to see that the intensity of the peak due to In-Sn nearest neighbours becomes lower when the temperature decreases and approaches the liquidus boundary indicating that indium and tin atoms start to separate in the melt.

CONCLUSIONS

XRD supplements thermal analysis and microscopic exami-

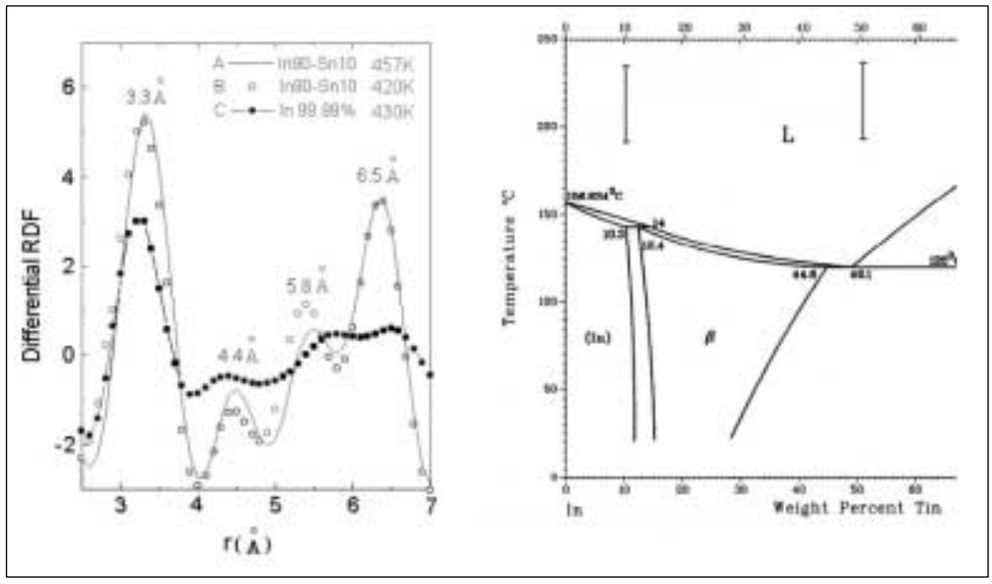

Fig.11- (Left) Differential RDF curves of In90-Sn10 alloy at 457 K (A) and 420 K (B), of pure indium (99.99 wt%) at 430 K (C). (Right) Phase diagram of the In-Sn system.

Fig.11- (Sinistra) Curve RDF differenziali della lega In90-Sn10 a 457 K (A) e 420 K (B) , di indio puro (99.99 peso%) a 430 K (C). (Destra) Diagramma di fase del sistema In-Sn.

nation in determining phase diagrams and permits, in addition, to find the crystal structures of solid phases. Some aspects of investigations on ordering transformations and determination of solvus curves have been described.
Experimental problems connected to high-temperature XRD have been discussed with particular attention to phase transformations which exhibit a fast kinetics.
The paper also showed that XRD offers the possibility to investigate structural transformations preceding and accompanying phase transformations. Melting and solidification of pure indium and of the In90-Sn10 alloy have been considered.

REFERENCES

1] B.D. Cullity, Elements of X-ray diffraction, Addison-Wesley Publishig Company, 1978, p.372.
2] H. Xiao and I. Baker, "The relationship between point defects and mechanical properties in Fe-Al at room temperature", Acta Met. Mater., 43 n.1, 1995, pp.391-396.
3] H. Doi, K. Hashimoto, K. Kasahara and T. Tsujimoto, "Site determination of third elements in TiAl compounds by X-ray diffractometry", Materials Transactions, JIM, 13, 1990, pp.975-982.
4] M. Kogachi, S. Minamigawa and K. Nakahigashi, "Determination of long range order and vacancy content in NiAl β' phase alloys by X-ray diffractometry", Acta Met. Mater., 40 n.6, 1992, pp.1113-1120.
5] A. Taylor, An introduction to X-ray metallography, Chapman and Hall, 1952, p.150.
6] H. Wang and E.A. Payzant, "Infrared imaging of temperature distribution in high-temperature X-ray diffraction furnace", Proc. of SPIE Conference, vol.3700, 1999, pp.377-385.
7] L. Margulies, M.J. Kramer, R.W. Mc Callum, S. Kycia, D.R. Haeffner, J.C. Lang, and A.I. Goldman, "New high temperature furnace for structure refinement by powder diffraction in controlled atmospheres using synchrotron radiation", Review of Scientific Instruments, 70, 1999, pp.3554-3561.
8] R. Montanari and G. Costanza, "XRD investigations on structural aspects of Indium melting", Proc. of the 1st International Symposium on Microgravity Research and Applications in Physical Sciences and Technologies, Sorrento 2000, pp.417-424.
9] P. Gondi, R. Montanari and G. Costanza, "X-ray characterization of Indium during melting", Advances in Space Research, 29/4, 2001, pp.521-525.
10] G. Costanza, F. Gauzzi and R. Montanari, "Melting and solidification of Indium: a structural investigation", Journal Microgravity Materials Science (in print).
11] A.R. Ubbelohde, The Molten State of Matter, Wiley Interscience Publication, 1978.
12] Y. Kishimoto and S. Tanigawa, "The study of thermal equilibrium defects and melting in indium by two-parameters correlation measurements of positron annihilation", in Point Defects and Defect Interactions in Metals, Eds. J. Takamura, M. Doyama and M. Kiritani, North-Holland Publishing Co., Amsterdam, 1982, pp.281-283.
13] P.H. Dederichs, "Diffuse scattering from defect clusters near Bragg reflections", Phys. Rev. B, 4 n.4, 1971, pp.1041-1050.
14] F.J. Humphreys and M. Hatherly, Recrystallization and related Annealing Phenomena, Pergamon Press, 1996, p.321.

ABSTRACT

STUDI SULLE TRASFORMAZIONI DI FASE MEDIANTE DIFFRATTOMETRIA X AD ALTA TEMPERATURA

PAROLE CHIAVE
Diffrattometria con raggi X ad alta temperatura, Diagrammi di fase, Trasformazioni di fase, Fusione, Solidificazione

Lo studio sperimentale dei diagrammi di stato è fondamentalmente basato su analisi termica, microscopia e diffrazione dei raggi X (XRD). Queste tecniche presentano diversa sensibilità in porzioni diverse dei diagrammi. I migliori risultati nella determinazione delle curve di liquidus e solidus, delle linee di peritettico ed eutettico si ottengono con l' analisi termica. Le curve di solvus, le orizzontali peritettoidi ed eutettoidi si studiano più facilmente con misure XRD e microscopia.
Questo lavoro fornisce alcuni esempi di applicazioni XRD nella determinazione dei diagrammi di fase discutendo i problemi sperimentali connessi. Viene inoltre mostrato come tecniche XRD ad alta temperatura possano essere impiegate per studiare aspetti strutturali delle trasformazioni, sia con la presen-

za di fasi solide che liquide.

XRD e la determinazione dei diagrammi di fase

Fig.1, riportata da Cullity [1], richiama alcuni criteri generali mostrando gli spettri di leghe di un ipotetico sistema A-B con diversa composizione nelle regioni monofasica e bifasica. Si riportano poi alcune classiche applicazioni della diffrattometria X allo studio dei diagrammi di fase.

Ordinamento in soluzioni solide sostituzionali

La presenza nello spettro di diffrazione di righe di superstruttura indica che in una porzione di materiale c'è ordine a lungo raggio. Dal rapporto tra le intensità integrate di una riga di superstruttura e della corrispondente riga fondamentale si calcola il parametro di ordinamento S.

Mediante diffrazione RX si può inoltre determinare la dimensione media L dei domini ordinati, la frazione di siti occupati da una specie atomica nell'anti-reticolo [2], l'occupazione reticolare di terzi elementi [3], la concentrazione di vacanze nelle soluzioni solide ordinate difettive [4]. La grande potenzialità della diffrattometria X negli studi strutturali è mostrata nell'esempio di figg.2-3 riguardante il sistema Al-Ni [5].

Le intensità delle righe di superstruttura di una lega binaria sono proporzionali a $(f_A-f_B)^2$, dove f_A e f_B sono i fattori di diffusione atomica dei metalli A e B. Se i numeri atomici Z_A e Z_B dei due metalli sono molto vicini, queste righe possono avere intensità così debole da non essere rilevabili. Questo inconveniente può essere superato usando una lunghezza d'onda λ prossima allo spigolo di assorbimento di una delle due specie atomiche.

Curve di solvus

I metodi XRD per determinare le curve di solvus sono due: il metodo della fase che scompare ed il metodo parametrico. Con riferimento a fig.4 (sinistra) per determinare il solvus bisogna trovare il punto x a varie temperature. Il metodo della fase che scompare consiste nel misurare il rapporto I_β/I_α tra due riflessioni delle fasi α e β per un certo numero di leghe con contenuto di B decrescente. Estrapolando a zero il rapporto I_β/I_α si trova x. La precisione del metodo dipende principalmente dalla sensibilità con cui si possono rilevare piccole quantità di fase β nella lega. Questa non è costante in quanto dipende dalla coppia di elementi A e B. Se i numeri atomici Z_A and Z_B sono vicini è possibile rilevare una quantità di seconda fase di circa 1%; se essi differiscono di 70 o più unità anche 50% può produrre intensità trascurabili, in questo caso il metodo è del tutto inutile. In ogni caso, se la regione $(\alpha+\beta)$ è molto stretta, dell' ordine di pochi per cento, il punto x potrà essere determinato sempre con sufficiente precisione essendo simili le composizioni delle due fasi. Il metodo parametrico si basa sul fatto che nella regione monofasica il parametro reticolare varia con la composizione mentre è costante nella regione bifasica, cosìcchè la curva parametrica mostra due rami ben distinti (vedi fig.4 destra). Il punto x viene determinato dall' intersezione dei due rami.Questo metodo può essere anche usato per trovare il confine tra una regione monofasica e una bifasica in un diagramma ternario (fig.5).

Diffrattometria X ad alta temperatura

Spesso le misure diffrattometriche vengono eseguite su leghe portate all' equilibrio ad alta temperatura e poi temprate per congelarne la struttura. Se, nonostante il raffreddamento rapido, la lega si trasforma è indispensabile eseguire le misure direttamente ad alta temperatura.

Se la cinetica di trasformazione è relativamente lenta, gli esperimenti possono essere fatti mediante una camera ad alta temperatura montata su un diffrattometro standard. Se invece la cinetica di trasformazione è molto rapida, le soluzioni possibili sono due: 1- usare rilevatori veloci; 2- operare mediante T.A.D..

L' apparato T.A.D. consiste di un contatore curvo in grado di registrare sia il numero di fotoni X che la posizione angolare in cui essi entrano e di un analizzatore multicanale (fig.6a). Ogni canale corrisponde ad un determinato intervallo angolare e qui si accumulano i relativi conteggi. La figura di diffrazione si ottiene visualizzando la memoria del multicanale. La risoluzione angolare ($2\theta=0.03°$) è comparabile con quella di un diffrattometro standard (0.005°) ma l' intero spettro di diffrazione si può ottenere in pochi secondi. Fig.6 b) mostra un' apparecchiatura T.A.D. con camera ad alta temperatura.

In alcuni casi, come nello studio della trasformazione peritettica, è consigliabile operare in trasmissione secondo lo schema sperimentale riportato in ref. [7].

Effetti precursori delle trasformazioni di fase

Un aspetto interessante delle trasformazioni di fase sono le variazioni strutturali che le precedono. Come esempio si riportano alcuni risultati [8-10] riguardanti la fusione e solidificazione dell'indio e della lega In90-Sn10.

Lo spettro registrato al punto di fusione T_M è la sovrapposizione delle figure di diffrazione dovute a solido e liquido. Come mostrato in fig.7 a), i due contributi possono essere separati e poi esaminati.

La funzione di distribuzione radiale (RDF) ottenuta dal contributo del liquido è riportata in fig.7 b).

Si osserva che la distanza media degli atomi primi vicini nel liquido, corrispondente al primo massimo della RDF, è molto vicina a quella di primi e secondi vicini nel solido, indicata dalle barre.

Confrontando lo spettro registrato a 428 K, subito sotto T_M, ed il contributo della fase solida alla figura di diffrazione a T_M si osservano alcune importanti variazioni (fig.8): 1- la riga {101}, assente nello spettro a 428 K, appare at 429 K; 2- il profilo del picco {002} è allargato soprattutto nella parte bassa; 3- durante la fusione il picco {002} si sposta verso angoli più bassi.

Fig.9 mostra come al punto di fusione si registra un improvviso incremento del volume della cella unitaria ΔV pari a 0.35 $Å^3$. Questo fenomeno è stato attribuito ad un aumento anomalo della concentrazione di vacanze, stimato come $\Delta C = 6.74 \times 10^{-3}$ [10].

Come dimostrato anche da altre ricerche [12], l' incremento abnorme di vacanze a T_M favorisce fenomeni di aggregazione con formazione di difetti complessi quali anelli di dislocazioni, che provocano allargamento del profilo dei picchi XRD nella parte bassa [13]. Una grande densità di vacanze aumenta inoltre la mobilità dei bordi di grano e quindi può spiegare la repentina variazione di tessitura evidenziata dalla comparsa del picco {101} al momento della fusione del metallo.

Fig.10 a) mostra gli spettri XRD registrati durante il raffreddamento fino a T_M dove il primo solido si forma con una forte orientazione [211]. Le RDF ottenute dagli spettri in a) sono riportate in b).

Lo sdoppiamento del secondo massimo di RDF prima dell' inizio della solidificazione indica la formazione di aggregati atomici con distanze medie comparabili con quelle dei primi vicini nei piani {211}, che risulteranno essere paralleli al liquido. Pertanto anche nella solidificazione, così come nel caso della fusione, sembrano esserci strette correlazioni tra le strutture delle due fasi.

Indicazioni simili si ottengono anche esaminando la solidificazione della lega In90-Sn10. In fig.11 (sinistra) la curva RDF differenziale della lega In90-Sn10 acquisita a 457 (A) e 420 K (B) viene confrontata con quella dell' indio 99.99% (C) a 430 K. Come mostrato nel diagramma di fase, 420 K per In90-Sn10 e 430 K per l'indio sono temperature appena superiori a quelle in cui comincia a formarsi il primo solido. Le curve A and B mostrano un picco a 4.4 Å dovuto a primi vicini In-Sn, che è di intensità trascurabile nella curva C. La sua intensità decresce con la temperatura ad indicare che avvicinandosi al liquidus gli atomi di indio e stagno iniziano a separarsi nel fuso.